Experimental Analysis of Thermomechanical Properties of Innovative Heat Treated Metal Matrix Composites Processed by Additive Manufacturing for Space Rocket Applications

Original
Experimental Analysis of Thermomechanical Properties of Innovative Heat Treated Metal Matrix Composites Processed by Additive Manufacturing for Space Rocket Applications / Lusicini, Delio; Crachi, Matteo; Sesana, Raffaella; Delprete, Cristiana; Sicignano, Nicola. - In: JOURNAL OF MATERIALS ENGINEERING AND PERFORMANCE. - ISSN 1059-9495. - ELETTRONICO. - 34:17(2025), pp. 19824-19839. [10.1007/s11665-025-11165-x]

Publisher:
Springer

Published
DOI:10.1007/s11665-025-11165-x

JMEPEG (2025) 34:19824–19839
https://doi.org/10.1007/s11665-025-11165-x

1059-9495/$19.00

ORIGINAL RESEARCH ARTICLE

Experimental Analysis of Thermomechanical Properties of Innovative Heat Treated Metal Matrix Composites Processed by Additive Manufacturing for Space Rocket Applications

Delio Lusicini, Matteo Crachi, Raffaella Sesana, Cristiana Delprete, and Nicola Sicignano

Submitted: 18 June 2024 / Revised: 8 January 2025 / Accepted: 1 February 2025 / Published online: 21 April 2025

In aerospace industry, additive manufacturing (AM) is widely used with innovative materials with high thermal conductivity and high resistance to produce liquid rocket engines. The aim of this study is to analyze the effects of heat treatments on properties and microstructure of an innovative metal matrix composite, Cu174PH, and to optimize the process in terms of thermal and mechanical properties. Seven heat treatments were applied to Cu174PH AM specimens, and their influence was evaluated through hardness tests, thermal conductivity measurements, and CT scans. Results show that optimal heat treatments significantly enhance the material's properties, achieving a thermal conductivity of 78.99 W/mK and a hardness of 197 HV. Specifically, three treatments (age hardening at 500 °C for 10 h, 600 °C for 10 h, and 700 °C for 10 h) were identified as optimal, balancing hardness and conductivity. The findings demonstrate the potential of Cu174PH as a high-performance material for aerospace applications, particularly in liquid rocket engine thrust chambers, offering an alternative to conventional alloys like CuCrZr and Inconel 718.

Keywords additive manufacturing, copper, heat treatment, mechanical testing, metal matrix composite, thermal analysis

1. Introduction

In the context of New Space Economy research, liquid rocket engines require high thermal conductivity and high-strength materials. The complex geometries resulting from designing process suggest to process the component by means of Additive Manufacturing (AM). The interest in AM thrust chambers is rapidly growing in the space industry, as evidenced by numerous developments and multiple flight applications (Ref 1). Liquid rocket engine combustion chambers operate in high heat flux environments, necessitating the use of high-strength, high-conductivity alloys to effectively cool the thrust chamber walls with high-pressure propellant or oxidizer. For this reason, copper alloys are mainly used for thrust chambers (Ref 1).

High-performance materials and complex designs are utilized to enhance efficiency by reducing costs, lead times, and component mass while adhering to budget and schedule constraints for commercial orders or mission requirements. Thanks to the design freedom of AM, material distribution can be optimized, allowing for mass reduction while maintaining performance requirements. Components consisting of several parts can be produced as a single object, this reduces cost and potential failure modes across joint. AM, compared to traditional techniques, uses less stock material by mass, leading to lower manufacturing costs and simplified recycling and reprocessing. It is possible to utilize a mix of different alloys or newer ones that are challenging to produce using traditional methods (Ref 1). Component quality and properties can be influenced by process parameters such as power, scan speed, hatch spacing, or track overlap. All aerospace manufacturing must comply with stringent quality check, including Quality Systems - Aerospace SAE AS9100 and standards like MSFC-STD3716 for AM Spaceflight Hardware and NASA Standard 6030. The most used AM technologies in the space sector are Laser Powder Bed Fusion (LPBF) and Direct Energy Deposition (DED). While with the first it is possible to produce components with better characteristics, with the second it is possible to produce larger volumes (Ref 2).

Despite the numerous advantages of AM, the material properties of AM components might not consistently be ideal in their initial as-built condition. Consequently, post-processing steps become imperative. Among the various post-processing techniques, heat treatment assumes a pivotal role in improving the final properties of metallic materials. This is particularly crucial for tailoring the physical and structural properties of parts to meet application requirements (Ref 3). In the context of metallic materials, heat treatment involves a controlled heating and cooling process designed to modify the microstructure (Ref 4), thereby improving physical and/or mechanical properties. Key microstructural features influencing these properties in a given alloy are grain size, morphology, grain boundary

Delio Lusicini, Matteo Crachi, Raffaella Sesana, and **Cristiana Delprete**, DIMEAS, Politecnico di Torino, Corso Duca degli Abruzzi, 24, 10129 Torino, TO, Italy; and **Nicola Sicignano**, Sophia High Tech, Via Malatesta, 30A, 80049 Somma Vesuviana, NA, Italy. Contact e-mail: delio.lusicini@polito.it.

characteristics, constituent phases, inclusions, dislocation density, and residual stresses. The microstructure of metals, however, greatly depends on the AM technology used, alloy composition, and process parameters (Ref 3). Consequently, a meticulous tailoring of all these microstructural features is essential when examining the impacts of heat treatment to comprehend the underlying mechanisms governing the resultant properties (Ref 3).

In (Ref 5), age hardening on the AM copper alloy CuCrZr has resulted in positive effects on both hardness and thermal conductivity. Wallis et al. began their analysis with the assumption that higher aging temperatures and longer aging times would enhance hardness and thermal conductivity, as precipitation behavior depends on both temperature and time. The CuCrZr samples underwent aging hardening from 400 to 580 °C for 10-300 minutes. The increase in temperature and exposure time firstly led to an increase in hardness until reaching a maximum value, reached between 450 and 500 °C, after which a decrease caused by the over-aging is observed. The thermal conductivity curve showed a constant general trend which increases as the temperature and aging time increase. The microstructure of laser fused age hardened parts is similar to that of as-built parts. Nevertheless, for CuCrZr it has been demonstrated that the formation of coarse precipitations is hindered by age hardening, resulting in enhanced mechanical properties (Ref 5). In (Ref 6) Cu-Ni-Sn-P alloy underwent homogenization heat treatment at 820 °C for 12 hours, followed by age hardening at 400 °C for 0.25-4 hours. The results in terms of thermal conductivity revealed an approximately 12% increase with aging for 0.5 hours and an approximately 30% increase with aging durations of 2 and 4 hours (with no significant differences between the latter two). The enhancement in conductivity was attributed by the authors to the presence of Ni, this results in scattering of free electrons inside the Cu matrix, dispersing into $(Cu, Ni)_3P$ precipitates during age hardening. Extending the aging duration to 4 hours did not result in additional Ni enrichment due to the saturation of precipitate sizes after 2 hours, and consequently, there were no significant changes in thermal conductivity's value (Ref 6).

In (Ref 7) samples of 17-4PH underwent to various heat treatments at a temperature range of 480-620 °C for a duration of 0.5 to 8 hours. By age hardening at 480 C for 1 hour, the maximum hardness value was attained; prolonging aging time at the same temperature does not involve a relevant variation of hardness value. With age hardening at 565 °C and 620 °C an initial increase in hardness value was followed by a considerable decrease in hardness value after 0.5 hours (Ref 7). In (Ref 28), in the as-built condition, LPBF 17-4PH has higher hardness than conventional materials, attributed to the smaller grain sizes and refined martensitic structure, which impede dislocation movement through grain boundary strengthening mechanisms. Aging at 482 °C for 1 hour (H900) yields maximum hardness values of 469 HV for conventional material and 534 HV for LPBF material. This increase is due to the precipitation of hard phase particles within the martensitic matrix. Aging at 593 °C for 4 hours (H1100) reduces hardness to 367 HV for both material types, due to over-aging phenomena where coalescence of hard phase particles diminishes their effectiveness in hardening the matrix (Ref 28). In (Ref 35), 17-4 PH stainless steel processed via Laser Powder Bed Fusion (LPBF) underwent the same heat treatments (H900 and H1100). Starting from an as-built hardness of 296.18 HV, the hardness values reached 413.21 HV and 386.33 HV following H900 and H1100 treatments, respectively. In (Ref 34), however, the material was subjected to shot peening prior to heat treatment, achieving an initial hardness of 410 HV, which further increased to 650 HV with H900 and 440 HV with H1100.

Different studies have been carried out on LPBF maraging steel 300 in order to find a heat treatment to improve mechanical properties. In (Ref 8), it resulted that the aging parameters which developed the maximum hardening is 5 hours at 480 °C, and a hardness of 58HRC was achieved. In (Ref 9) a similar value of hardness (57 HRC) with a longer heat treatment, 500 °C for 5 hours is obtained. In (Ref 10) the optimum heat treatment plan is identified 5 h at 460 °C. In (Ref 11) a hardness measurement campaign was performed on solution treated and aged LPBF MS300 in a large range of time (from 0.25 to 25 hours) and of temperature (from 440 to 560 °C). The maximum (700 HV) was reached after 10 hours at 480 °C. In (Ref 12) the effects of a larger range of hardening parameters is investigated and the peak value of hardness (650 HV) is found after 8 hours at 460 °C. It is possible to summarize that in each of the cited studies, for each temperature of heat treatment a peak is reached for a particular duration after which over-aging begins (Ref 13). In (Ref 29) is investigated the effect of the as-built microstructure on the martensite to austenite transformation in an 18Ni maraging steel produced via LPBF. Using in situ synchrotron X-ray diffraction, the study examines phase transformation kinetics during continuous heating and isothermal tempering. The results show that at slow heating rates (0.167 °C/s), the intercritical $\alpha + \gamma$ range of the as-built microstructure expands compared to a solution-treated sample. However, at heating rates of 5 °C/s or higher, the massive reversion mechanism dominates, rendering the initial microstructure irrelevant. During isothermal tempering, the minor amount of retained austenite and slight compositional partitioning in the as-built state do not significantly alter austenite reversion kinetics or the ability to achieve thermodynamic equilibrium compared to a solution-treated sample. Similar volume fractions of reverted austenite are achieved after 2200 seconds of tempering through the intercritical $\alpha + \gamma$ field for both initial microstructures. Additionally, thermal stability of austenite is fully observed after cooling from tempering temperatures below 670 °C for both initial microstructures. Partial transformation of austenite to martensite occurs during cooling after tempering at 670 °C. The study provides insights for designing heat treatments for LPBF-produced maraging steels to enhance mechanical properties. In (Ref 37), the impact of heat treatment on the mechanical properties of maraging steel 18Ni (300) was analyzed, focusing on hardness, tensile strength, and ductility. The primary heat treatments examined included temperatures of 470 °C, 510 °C, and 530 °C, each promoting the precipitation of reverted austenite (γ). At 470 °C, after 24 hours of heat treatment, the steel achieves its highest hardness of 620 HV and a tensile strength of 2100 MPa, with a moderate amount of reverted austenite (3%). This low austenite content ensures that the steel remains strong and resistant to deformation, with minimal impact on ductility. At 510 °C, after a shorter duration of 3 hours, the steel reaches a hardness of 600 HV and a tensile strength of 2050 MPa. The amount of reverted austenite increases to 9%, which enhances the steel's toughness and ductility, making it more resistant to fractures. However, the slight reduction in hardness and strength compared to the 470 °C treatment reflects a trade-off for increased toughness. At

530 °C, the steel reaches 580 HV after just 20 minutes of heat treatment. This rapid heat treatment results in the highest amount of reverted austenite (14%), which significantly improves ductility and toughness, but reduces both hardness and tensile strength to 2000 MPa. The results indicate a clear trade-off between hardness and ductility. Lower temperatures (e.g., 470 °C) promote maximum hardness and strength but require longer treatment times, while higher temperatures (e.g., 530 °C) lead to increased ductility and toughness at the cost of hardness and strength. The balance between these properties allows the material to be tailored for specific applications, depending on whether higher strength or greater impact resistance is needed.

In the study (Ref 14), LPBF H13 hot work tool steel underwent two distinct heat treatment procedures. The initial procedure consisted of austenitizing at 1020 °C for 70 minutes, followed by quenching and double tempering at 585 °C for 2.5 hours. The second procedure involved direct tempering of the as-built specimens two times at 585 °C for 2.5 hours. The first treatment schedule resulted in a thermal conductivity increase ranging from 11% to 24%, depending on the initial density, while the second treatment yielded a rise of 6% to 15%. In (Ref 38), the heat treatments performed on H13 tool steel significantly impacted both hardness and compressive strength. The study compared four different heat treatment routes: direct tempering (T), double tempering (TT), austenitization followed by quenching and tempering (QT), and stress relief followed by austenitization, quenching, and tempering (SRQT). In terms of hardness, the austenitized samples (QT and SRQT) demonstrated higher hardness levels compared to the directly tempered (T) and double-tempered (TT) samples at the same tempering temperatures. For instance, the quenched samples (QT and SRQT) reached hardness values around 570 HV (573 HV for QT and 567 HV for SRQT), which were similar to the hardness of the as-built (AB) sample at 564 HV. However, the stress-relieved samples exhibited a significant drop in hardness, reaching 396 HV, which was even lower than the hardness of the samples tempered at 650 °C. The double-tempered (TT) route resulted in slightly lower hardness than the austenitized routes but still retained considerable hardness, making it a good option for applications requiring a balance of toughness and hardness. Compressive strength followed a similar pattern to hardness, with the QT and SRQT samples showing higher strength than the T and TT routes. The austenitized samples (QT and SRQT) displayed a compressive strength approximately 500 MPa higher than that of the directly tempered and double-tempered specimens. As the tempering temperature increased, the compressive strength decreased, which is typical behavior for Cr-alloyed tool steels during tempering. Higher tempering temperatures, such as 650 °C, reduced the material's strength but enhanced its ductility and toughness

Despite various ongoing research efforts addressing heat treatment for materials produced by means of AM, defining the optimal heat treatment conditions for many AM alloys remains an ongoing challenge. This issue is emerging as a significant topic in AM research, particularly regarding innovative materials, due to its profound industrial importance (Ref 3).

The present study aims at investigating the effect of heat treatment on Cu174PH6535, a new Copper-Maraging steel metal matrix composite (MMC) material processed by LPBF AM. In particular, the goal is to identify the heat treatment configuration with which the metal matrix composite material can achieve the best compromise between mechanical and thermal behavior. The powder of Cu174PH6535 is pre-processed by a mixing process from powder of Cu and of 17-4PH.

MMCs are engineered materials created by combining a metallic matrix with reinforcing materials to achieve customized properties, leveraging the strengths of both components (Ref 30, 41). These composites exhibit superior mechanical and thermal properties over a wide temperature range, making them suitable for demanding applications (Ref 30, 32). Traditional metal materials often suffer from limitations such as low specific strength and poor corrosion resistance, which MMCs effectively address through the incorporation of strengthening particles like ceramics or rare earth elements (Ref 31). LPBF has shown significant advantages over conventional powder metallurgy methods in processing metal powders due to its point-by-point consolidation and free-form fabrication capabilities (Ref 30). Despite this, the application of SLM in fabricating three-dimensional MMC parts remains underexplored, highlighting a need for further research in this area (Ref 30). The introduction of laser-assisted additive manufacturing (AM) techniques has opened new avenues for the development of MMCs, enabling the design of materials based on desired properties rather than passive optimization post-production (Ref 31, 40). This proactive approach, combined with advancements in material selection and process control, is expected to enhance the efficiency of developing new MMCs for AM (Ref 31). In (Ref 36), a MMC was developed by blending TiC powders (5 Wt.%) with AISI 420 powders, which were subsequently processed via LPBF. The study's optimal processing parameters resulted in a significant increase in hardness, from 196 HV in AISI 420 to 592.24 HV in the MMC. It was observed that the TiC reinforcement particles, distributed along the grain boundaries of the matrix, formed a decentered ring-like structure. This configuration potentially enhances resistance to indentation compared to the original matrix. Furthermore, an increase in ultimate tensile strength (UTS) was recorded, rising from 1050 MPa to 1452.5 MPa. This improvement is attributed to the size and distribution of TiC particles, which can enhance the ductility of the composites by inhibiting crack formation at the grain boundaries. This inhibition is due to the martensitic transformation of large particles and the prevention of interfacial decohesion. In (Ref 39), is examined the impact of TiB2 nanoparticles on the properties of 316L stainless steel in SLM-processed nanocomposites, designated as SMC-5 (5% TiB2), and SMC-10 (10% TiB2). The addition of TiB2 nanoparticles significantly enhances the yield strength across all temperatures tested, with the highest gains observed in SMC-10 due to improved grain refinement that hinders dislocation movement. At room temperature, the presence of TiB2 restricts the movement of planar slip bands, thus increasing strength but decreasing ductility, particularly in SMC-10. This reduction in ductility is more pronounced as the volume percentage of TiB2 increases. Elevated temperature tests at 600 °C reveal increased brittleness in both composites, exacerbated by the transformation of delta ferrite into the brittle sigma phase and the spinodal decomposition of ferrite, which leads to reduced toughness. Conversely, at temperatures of 700 °C and above, the composites show enhanced ductility, indicating that the negative effects observed at 600 °C are mitigated at higher temperatures. This behavior suggests a complex interplay between strength and ductility in the presence of TiB2, where higher temperatures alleviate the brittleness induced at intermediate temperatures.

Table 1 Carpenter Additive 17-4 PH powder chemical composition

Fe	C	Mg	P	S	Si	Cr	Ni	Cu
Balance	0-0·07	0-1·00	0-0·04	0-0·03	0-1·00	15·00-17·50	3·00-5·00	3·00-5·00

The study underscores the potential of TiB2 as a reinforcement in 316L stainless steel, offering a means to tailor mechanical properties through strategic control of nanoparticle content and processing conditions.

However, laser-assisted AM processes also introduce challenges such as high porosity, residual stress, and geometric distortion in the final components (Ref 32). These issues necessitate post-treatment techniques, including heat treatment and hot isostatic pressing, to improve the microstructure and mechanical properties of MMCs (Ref 32). While extensive research has been conducted on post-processing regular metal alloys produced via AM, similar efforts for MMCs are still lacking, suggesting a critical area for future exploration (Ref 32). Additionally, the high cost of raw powder preparation and post-processing in laser-assisted AM processes has been identified as a significant barrier to their industrial adoption, underscoring the need for cost-reduction strategies to make these technologies more economically viable (Ref 32).

2. Material and Methods

2.1 Material

Cu174PH6535 is an innovative MMC material obtained by Sophia High Tech s.r.l. by mixing two different materials: 65% Pure Copper and 35% 17-4PH. PM-CU101P is a gas atomized copper powder, customized for laser melting applications made by Legor Powmet. The declared chemical composition is 99.9% copper (Ref 15). PowderRange 17-4 AR (17 4PH named from Carpenter Additive) is a martensite precipitation/age hardening stainless steel. The chemical composition provided by the powder supplier is presented in Table 1 (Ref 16).

To obtain powder of Cu174PH6535, the two different powders of Copper and 174PH are used. The POWMIX project (Ref 18) has the goal of an industrialization of advanced metal powder mixing process for the AM sector. The final aim is to obtain a homogeneous mix (on a micrometric scale) of metal powders. The technique consists of the dual action of a pressurized gas and a sound pressure field, to avoid the density instability during mixing phase. The acoustic field breaks the electrostatic forces between particles and ensures a stochastic distribution of the mixed powder composed by the different powders. The fluid bed mixing technique, integrated with that of the acoustic field, acts as a force supplying energy to the fluid phase which allows and/or optimizes the separation and aggregation between the different powder clusters (Ref 18).

The AM machine is a Concept Laser M2. The process parameters adopted by Sophia High Tech are based on internal know-how in AM and on a previous work on Inconel718-Cu pre-mixed (Table 2) (Ref 18). The "island" scanning strategy has been employed in the present study. Each layer is subdivided into smaller sections, scanned randomly with orthogonal scanning vectors of the adjacent islands. For subsequent layers, the sections are rotated by random angles in both x and y directions. (Ref 19).

Table 2 LPBF Process parameters

	General	Body	Contour
Fusion strategy	Island (5 mm length)	…	…
Layer thickness, mm	0.03	…	…
Hatch distance, mm	0.105	…	…
Spot size, mm	0.15	…	…
Scanning speed, mm/s	…	253	400
Power, W	…	200	180
Beam compensation, mm	…	…	0.075
Overlap factor, -	…	0.7	…

The DoE was designed for the thermomechanical characterization of Cu174Ph6535, with constant process parameters. In this study, only a subset of the specimens produced, marked as 1*, 2*, and 3* in Fig. 1D, were considered for the analysis of heat treatments.

The specimens used in this study are divided into three categories:

1. Seven specimens for microhardness tests, thermal conductivity tests, micrography analysis and porosity analysis (Fig. 1A). These are cylinders with a diameter of 12 mm and a height of 5 mm. They were obtained by sectioning taller cylindrical specimens (indicated as *1 in Fig. 1D) into multiple parts to achieve the desired height. They were produced with the cylinder base aligned with the xy printing plane. Each specimen was subjected to mechanical polishing using a sander machine. Initially, polishing was performed with water coolant and sandpapers of varying granulometries, ranging from 2500 to 4000 grit. Subsequently, a polishing cloth (Polilap) and abrasive paste (from 4 μm to 1 μm) were used. After polishing, an average surface roughness (Ra) of 0.06 μm was obtained.
2. Three dog bone specimens for tensile tests (Fig. 1B). These have an axial gauge length of 25 mm and a transverse gauge length (width) of 6 mm. They were produced by turning the cylindrical specimens indicated as *2 in Fig. 1D. These were manufactured with the specimen axis parallel to the xy printing plane.
3. Three specimens for compression tests (Fig. 1C) indicated as *3 in Fig. 1D. These are cylinders with a diameter of 10 mm and a height of 20 mm. They were manufactured with the specimen axis parallel to the xy printing plane and were machined with CNC in order to achieve parallelism between opposite flat surfaces.

2.2 Heat Treatment

The treatments have been carried out in a PID controlled oven. Every sample has been treated separately from the others due to the different duration and/or temperature of the heat treatment.

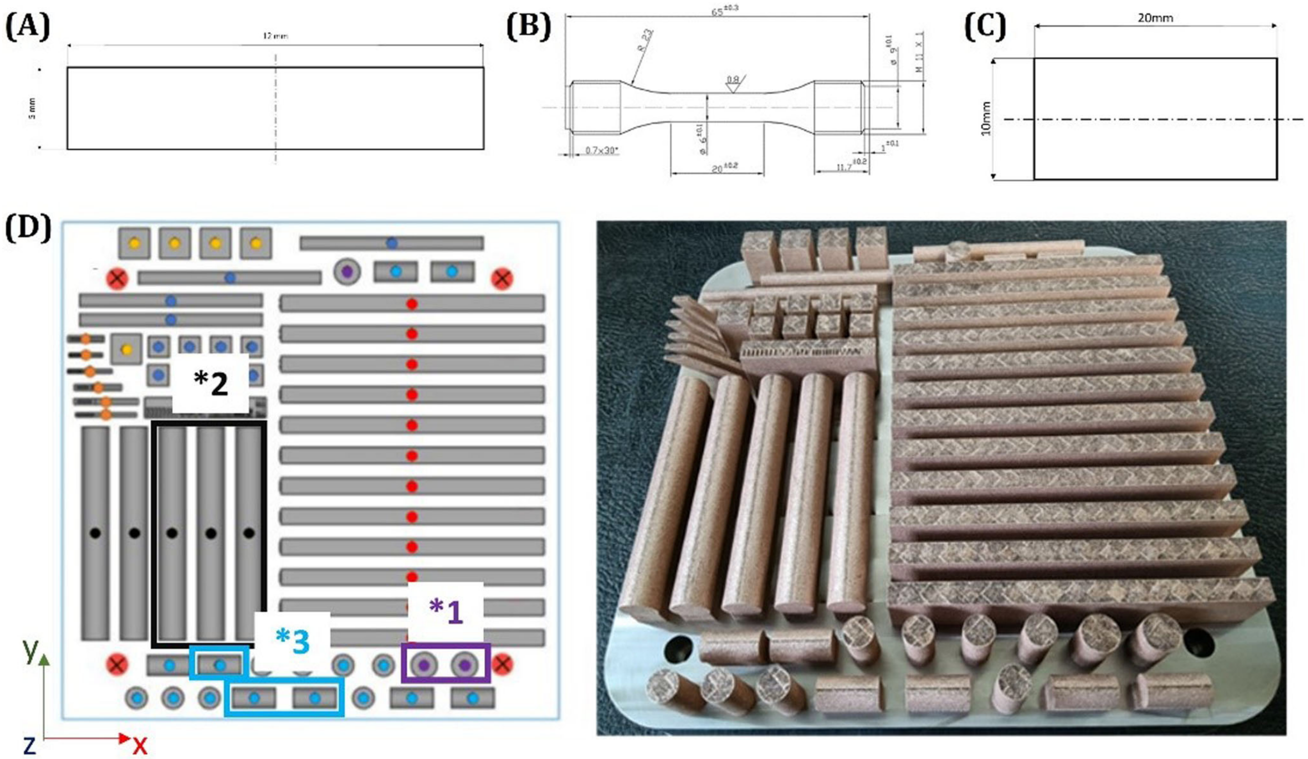

Fig. 1 Samples used for Harness/Thermal conductivity tests (A), tensile tests (B), compression tests (C) and general DoE (D)

The findings from the literature, summarized in the introduction, provided a basis for determining the optimal temperature range for heat treatments (Ref 6-8). The following heat treatments were then carried out:

- 400 °C for 10 hours;
- 500 °C for 10 hours;
- 700 °C for 10 hours;
- 800 °C for 10 hours.

The Heat Treatment (HT) temperature which provided the highest microhardness HV1 was selected to explore the influence of HT time and duration to 5 hours and age hardening at higher temperature for 10 hours was run. At the end, a water quenching was carried out to evaluate its effect on the MMC behavior.

Specimens were examined and tested. SEM and EDS were performed before and after HT to investigate the microstructure and composition of samples. Microhardness test, thermal conductivity and porosity measurements, tensile and compression tests were performed on the specimens as follows.

2.3 SEM - EDS Analyses

The equipment employed for micrographic and powder analysis comprises a Tescan VEGA scanning electron microscope (SEM) outfitted with an Ultim MAX SDD detector designed for chemical analysis (EDS). After attaching the copper and 174PH powders onto conductive supports, they were analyzed using a Scanning Electron Microscope (SEM). The images acquired with the SEM were then processed with ImageJ software to determine the area of the powders. Subsequently, the polished surfaces of the heat-treated specimens were also analyzed using SEM and EDS.

2.4 Microhardness

Microhardness HV1 has been evaluated with the microdurometer INNOVATEST NOVA 130 also integrated with the Impressions™ tester control. Microhardness tests were performed on the flat base of the specimen.

Data acquisition was performed according to Standard EN ISO 6507. For each sample 10 different measurements at room temperature were taken. Since there are not Standards designed to perform surface hardness measurements designed for AM samples, Standard designed for general purpose metallic samples were applied according to J. Slotwinski (Ref 20). According to BS EN ISO 6507, to ensure valid indentation, it is necessary to have a flat surface that has minimal surface roughness. For this reason, it has been inevitable to perform a surface finishing treatment on the surfaces of the samples before the test. Mechanical polishing was made with a sander machine, firstly with water coolant and with different granulometry sandpapers, from 2500 to 4000, secondly with a polishing cloth (Polilap) and abrasive paste (from 4 μm to 1 μm). After polishing, an average surface roughness Ra of 0.06 μm was obtained.

2.5 Thermal Conductivity and Porosity Measurements

Thermal conductivity test was run using a Hot Disk Thermal Constants Analyser, by means of the isotropic method. Specimens' geometry have been chosen according to Standard UNI 22007-2. Porosity analysis was carried out to quantify the influence of porosity on thermal conductivity. Other properties being equal, with increasing porosity, thermal conductivity decreases (Ref 21).

The Maxwell–Eucken model (Ref 21) models the thermal conductivity of biphase material:

$$k = \frac{k_1 v_1 + k_2 v_2 \frac{3k_1}{2k_1+k_2}}{v_1 + v_2 \frac{3k_1}{2k_1+k_2}}$$

where k_1 and v_1 are the conductivity and the volume fraction of the parent material, k_2 and v_2 are the conductivity and the volume fraction of the dispersed medium (pores), k are the global conductivity.

Assuming the pores as the dispersed medium, given k from Hot Disk measurement, v_2 and v_1 from CT scan acquisition, then k_1 that is the base material thermal conductivity is obtained.

$$k_1^2 \frac{2v_1}{k} + k_1 \left(-3v_2 + 3k_2 v_2 - 2v_1 + \frac{k_2}{k} v_1 \right) - k_2 v_2 = 0$$

The instrument used for porosity analysis is a customized CT scan produced by Fraunhofer IKTS. The acquisition parameters used are as follows: tube voltage 55 kV, tube current 150 μA, and scan time 75 minutes. The image resolution obtained is 0.012 χ 0.012 χ 0.012 mm. The images obtained with the CT scan machine are then analyzed with VG Studio Max software to obtain the volumetric fraction of porosity. The CT scan provides images in grayscale where porosities and solid material exhibit different shades of gray. The VG Studio Max software can evaluate these varying shades and automatically calculate the percentage of porosity relative to the total volume of the specimen.

2.6 Tensile and Compression Tests

The machine used for tensile and compression tests is an INSTRON 8801 hydraulic 100 kN. It is equipped with a bi-axial INSTRON extensometer to measure the Poisson ration. Test speed of 1 mm/min was set for tensile and compression tests, axial 25 mm gauge length, traversal 6 mm gauge length (width). The test has been performed at room temperature. Sample geometry for tensile test has been chosen according with ISO 6892, ASTM E8 and ASTM E21 (Figure 1B). During the tensile test, the load was applied parallel to the axis of symmetry of the specimens.

Compression test has been performed according to the ASTM E209, using cylindrical specimen (Figure 1C). During the compression test, the load was applied parallel to the axis of symmetry of the specimens.

Three compression tests and three tensile tests were run.

3. Results

3.1 SEM-EDS Analyses

The granulometric distributions of both Cu and 17-4PH powders were analyzed with aid of a SEM and the acquired images were processed with the ImageJ software. The results are reported in Table 3 and in Figure 2 the distribution of the powder particles area is plotted.

When comparing the powder of the two different materials it is possible to notice the different shape of the particles. While those of 17-4PH are very irregular, those of Cu are quite spherical: This leads to a greater smoothness of copper particles on the printing bed. Another difference is that the copper particles are slightly smaller. In both materials it can be seen a clear differentiation of particle size. The variations in shape and size between the powders of the two materials impact their flowability throughout the printing process. The segregation problem, as already reported in (Ref 17) is also related to different component densities and it affects all MMC, even when processed by other methods like powder metallurgy.

Table 3 Average and standard deviation of powder particle's area

	Average area, μm^2	D10, μm^2	D50, μm^2	D90, μm^2
Cu	264,5	44,9	241,1	480.63
17-4PH	304,4	53,3	277,7	565,1

Micrographic analyses using SEM were carried out both before and after heat treatment. After printing process, the micrography of Cu174PH6535 is characterized by a non-uniform distribution of material. Three main components can be observed (Fig. 3A):

- The darkest areas (1*): islands of 17-4PH (Figure 3B);
- The lightest areas (2*): areas consisting almost entirely of Copper (Fig. 3C);
- Intermediate zones (3*): areas characterized by a high Cu concentration along with elements derived from 17-4PH (Fig. 3D).

During the printing process, partial dissolution of the reinforcement particles (17-4PH) and subsequent interfacial reactions with the molten metallic matrix (Cu) lead to the formation of this hierarchical microstructure (Ref 33). This microstructure, characterized by a modified metallic matrix and residual reinforcement particles, result from the complex interplay between the original reinforcements and the matrix alloy (Ref 33). While these interfacial reactions can sometimes produce undesirable by-products that negatively affect the composite's properties, they also present opportunities for property enhancement (Ref 33). The remaining second-phase particles can act as nucleation sites during matrix solidification, promoting grain refinement and improving the mechanical properties of the composite (Ref 33). Additionally, the modified matrix may benefit from solid solution strengthening, due to elements released by the dissolved second phase, and precipitation hardening from new phases formed by the reactions between the matrix and reinforcement particles (Ref 33).

SEM images of samples after heat treatment are reported in Figure 4. In these pictures no significant differences are apparent in the micrographs following the various heat treatments.

The chromatic difference between the zones is due to the different concentrations of elements. This aspect has been analyzed in more detail thought the use of EDS. For each sample, EDS measurements were carried out on three different sites. At each site, both overall chemical composition measurements and point measurements on the 174PH islands were conducted. The purpose of this analysis is to identify the chemical composition of the islands of 17-4PH and compare it with what it would have if the specimen was composed exclusively of this steel. From this comparison it is possible to understand what elements have ended up in the copper matrix.

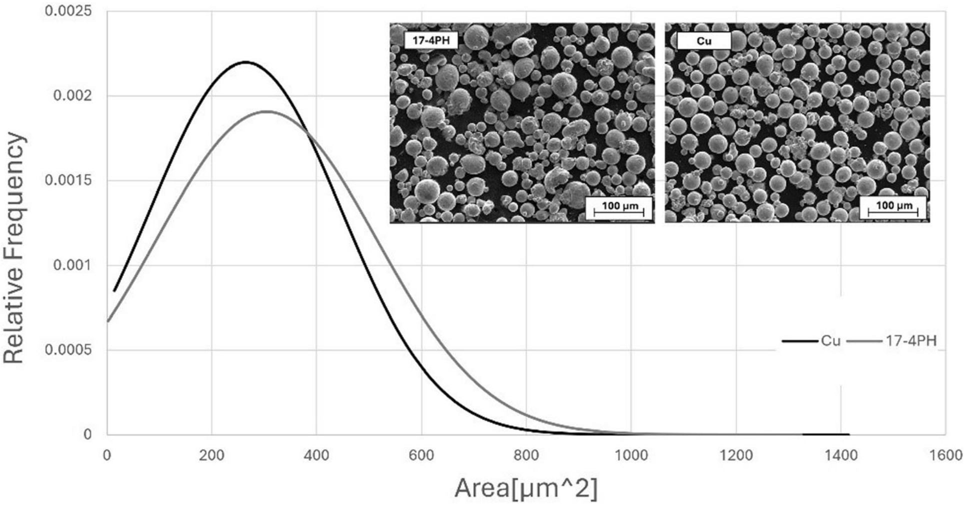

Fig. 2 Powder particle area distribution

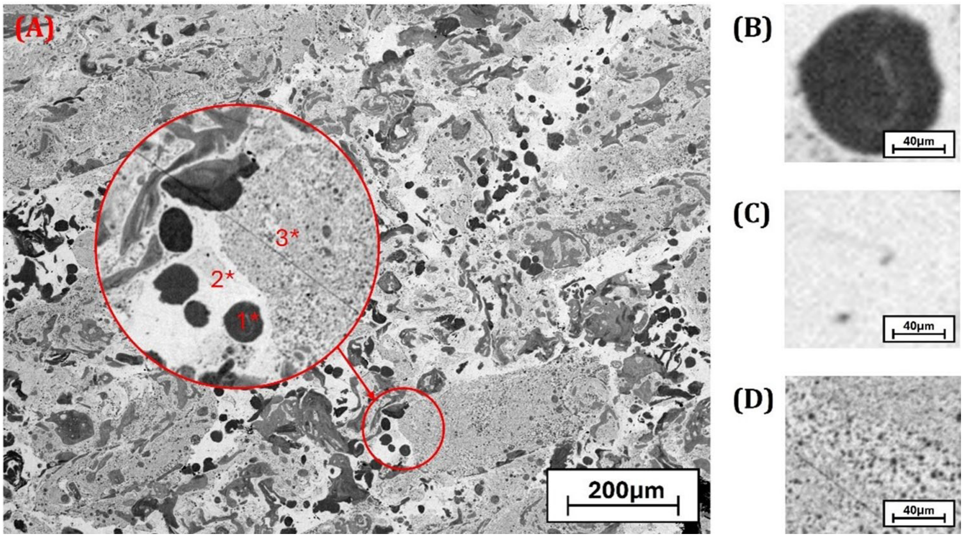

Fig. 3 Cu174PH6535 MMC as built micrography (A) total area; (B) islands of 174PH; (C) Copper matrix; (D) intermediate zones; plane xy

EDS analysis results on Cu matrix are presented in Figure 5. In Table 4, %Elements refers to weight percent (Wt.%) of all those elements which contaminate Cu, this value is the complementary of %Cu. In detail, the elements that make up %Elements are: Fe, Cr, Ni, Nb, Mn, Mo, Si, Co. Furthermore, there is a substantial difference between the distribution of elements obtained with heat treatments and those of as built. The %Cu increases with thermal treatments, thus meaning that the thermal treatments somehow ”cleans” the Cu from the other elements.

For each sample a transition zone (much clearer than the others) between the 17-4PH islands and the surrounding matrix was identified.

The results related to one of these transition zones are summarized in Figure 6 as an example. As expected, the clearest area is the one with the highest copper concentration.

3.2 Microhardness

Figure 7 and Table 5 show the results from microhardness tests. The hardness values of CuCrZr (from (Ref 5)) and 17-4PH (from (Ref 7)) after heat treatment are also reported. The highest value of microhardness is reached with the aging at 500 °C for 10 hours (197 HV). A similar result is obtained at 700 °C and the same duration (193 HV). Both quenching and age hardening at 600 °C leads to a reduction of hardness compared to as built.

The influence on microhardness of age hardening at 500 °C with a different duration was then investigated. Age hardening at 500 °C for 5 hours leads to hardness values close to those obtained at 500 °C for 10 hours.

3.3 Thermal Conductivity and Porosity Measurements

Table 6 shows the results obtained with CT scan for volume fraction of porosity and volume fraction of material. Due to the phenomenon of beam hardening, it appears that the samples are full of porosity on the external layer (Figure 8). Since this phenomenon leads to an incorrect evaluation of what is actually porosity, only the inner part of the samples was considered for porosity evaluation. The VG Studio Max software was accordingly set to analyze only the inner area.

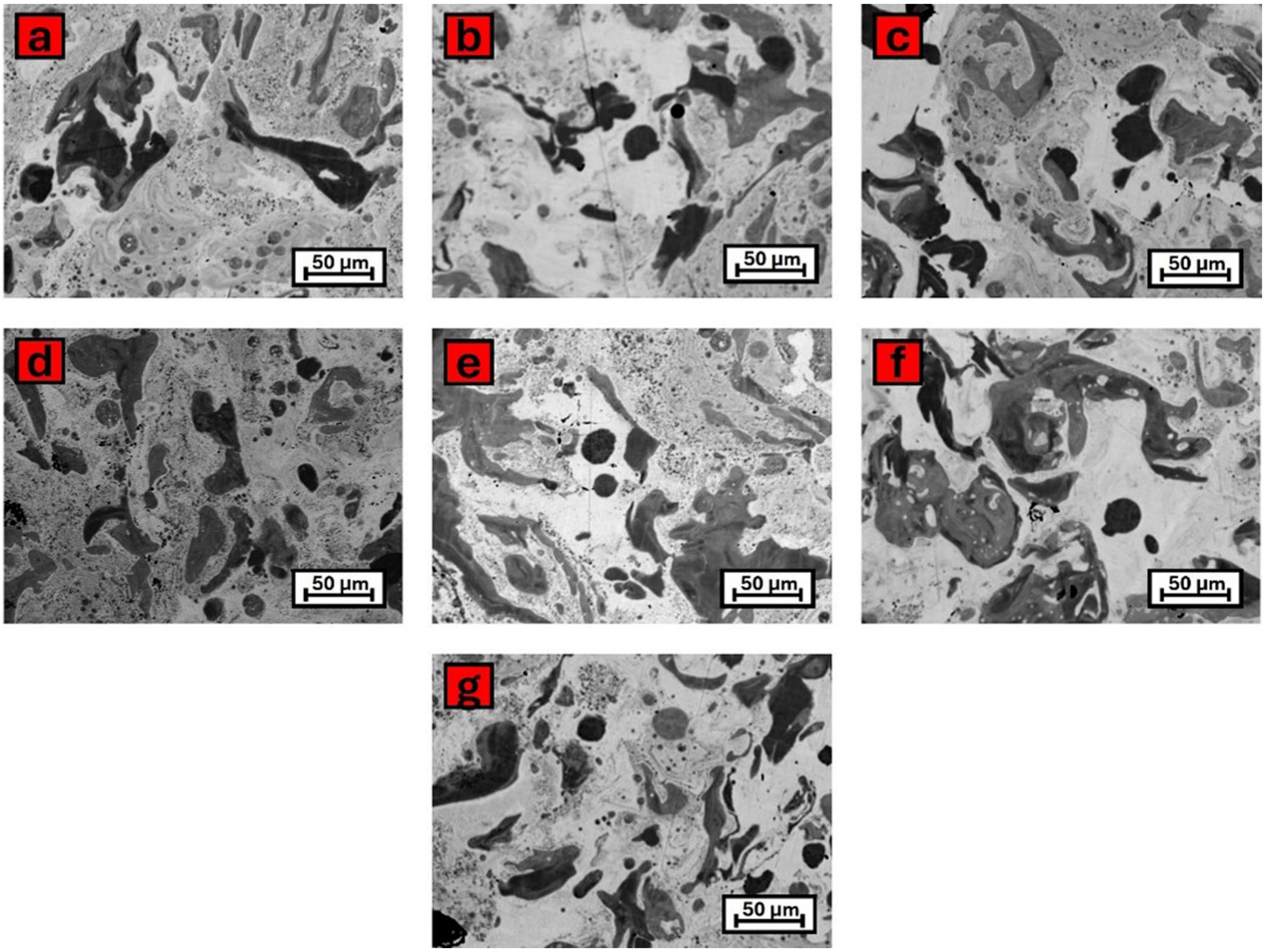

Fig. 4 SEM micrography (a) 400 °C-10 h; (b) 500 °C-10 h; (c) 600 °C-10 h; (d) 700 °C-10 h; (e) 800 °C-10 h; plane xy

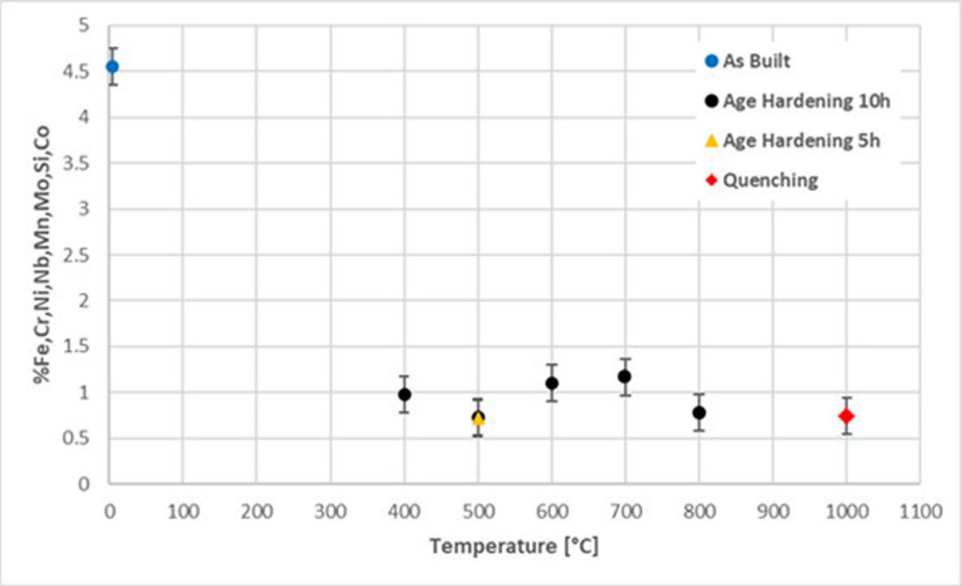

Fig. 5 Percentage of chemical elements for different heat treatments in Cu matrix

The thermal conductivity tests were carried out only along the *xy* plane because, from a previous study (Ref 18), it resulted that the values obtained for thermal conductivity along other directions are the same.

Figure 9 and Table 6 show the results from thermal conductivity tests. Table 6 also shows the thermal conductivity without porosity derived from hot disk thermal conductivity via Maxwell–Eucken model. For each of the analyzed specimen, an uncertainty of ± 10% was considered to take into account of some inaccuracies in the AM process:

- Due to the different flowability of copper powder and 17-4PH powder the printing process (before HT) produces specimens with different chemical composition depending on the point of the print volume in which they are located (Ref 18);
- The presence of porosity, which can be reduced by improving the process parameters, influences the thermal conductivity;
- HT generated surface oxidation of the specimen. If the oxide is not completely removed, it affects the measurement of thermal conductivity.

Table 4 Percentage of chemical elements for different heat treatments in Cu matrix

	Temperature °C	Time h	%Elements %
As built	0	0	4,55
Age Hardening	400	10	0,98
	500	10	0,73
	600	10	1,10
	700	10	1,17
	800	10	0,78
	500	5	0,72
Quenching	1000	0,5	0,74

Aiming at optimizing the heat treatment parameters which can provide the best properties to the AM MMC alloy, Figure 10 shows both the microhardness and thermal conductivity (porosity-adjusted) with varying HT. As the microhardness increases the thermal conductivity decreases and vice versa.

Then, for subsequent analyses the optimal treatments were chosen: age hardening for 10 h at 500 °C and 700 °C (highest microhardness values) and age hardening for 10 h at 600 °C (highest value of thermal conductivity).

Three tensile samples and three compression samples were subjected to the three selected heat treatments according to the hardness and thermal conductivity tests. These specimens were then subjected to tensile and compression tests.

3.4 Tensile and Compression Tests

The tensile and compression curves and results values of the as-built samples were taken from (Ref 18).

In Figure 11 the stress–strain curve of the tensile tests are plotted and the main results are summarized in Table 7. The data obtained show that:

- Maximum Stress: The highest values were obtained with 600 °C–10 h while the lowest values were obtained with 500 °C–10 h (these are very similar to those of 700 °C 10 h);
- Young's Modulus: The highest value was obtained with 700 °C–10 h while the lowest value was obtained with 500 °C–10 h;
- Flow Stress: The highest value was obtained with 600 °C–10 h (this is like that of 500 °C-10 h) while the lowest value was obtained with 700 °C–10 h;
- Failure Strain: The highest values were obtained with 600 °C–10 h while the lowest values were obtained with 700 °C–10 h ;
- Compared to as-built HT led to:

– A decrease in Young's modulus and Failure Strain;
– An increase in Maximum Stress;

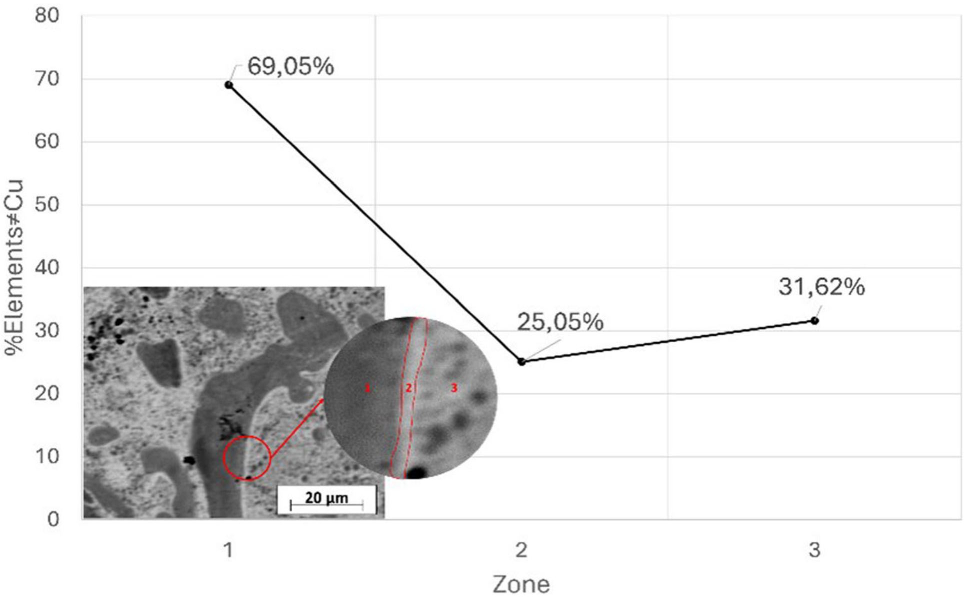

Fig. 6 Cu percentage in the transition zone; plane xy

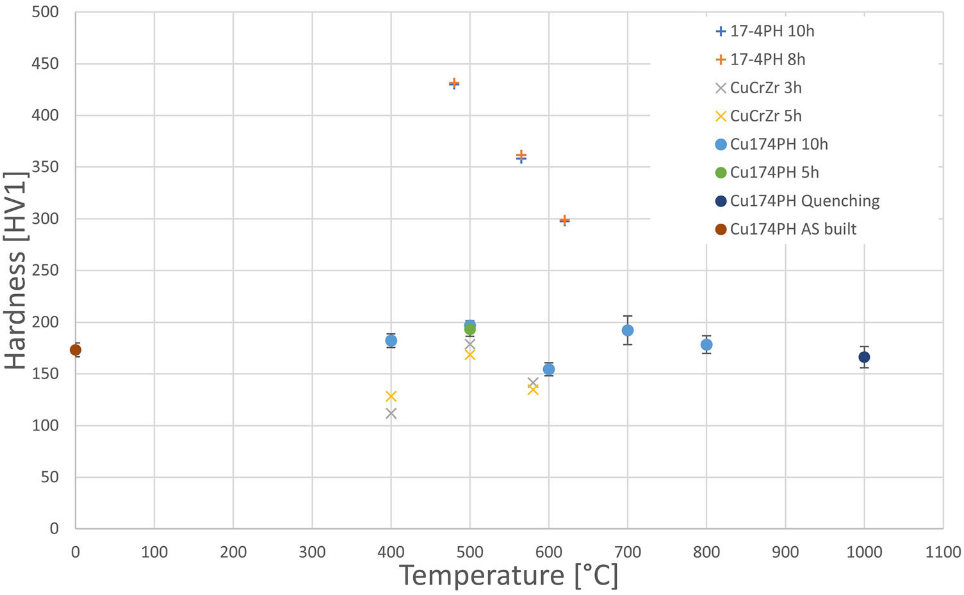

Fig. 7 Microhardness vs Heat Treatment temperature

Table 5 Microhardness HV1 results

	T, °C	t, h	Microhardness, HV	Std. Dev., -
As built	0	0	173.32	6.73
Age Hardening	400	10	182.17	6.61
	500	10	196.98	4.41
	600	10	154.44	6.31
	700	10	192.15	13.89
	800	10	178.29	8.51
	500	5	193.04	6.56
Quenching	1000	0.5	166.17	10.36

– An increase (500 °C–10 h and 600 °C–10 h) and a decrease (700 °C–10 h) in Flow Stress.

After tensile test the samples' failure surfaces have been analyzed with SEM (Figure 12). This analysis highlights the presence of voids and of some unmelted powder grains in all three samples: Both factors are causes of intensification of stresses.

In Figure 13 the stress–strain curve of compression tests are reported. The corresponding main results are summarized in Table 8. The data obtained show that:

- Maximum stress: The highest value was obtained with 500 °C –10 h while the lowest value was obtained with 700 °C–10 h (this is very similar to that of 600 °C–10 h);
- Young's Modulus: The highest value was obtained with 600 °C–10 h (this is very similar to that of 500 °C–10 h) while the lowest value was obtained with 700 °C 10 h;
- Compared to the as-built specimens, both the Maximum stress and the Young's Modulus are increased.

These increments are not as evident as in tensile tests. The elastic modulus does not show the decrement observed in tensile tests.

4. Discussion

The influence of HT on microhardness is pointed out in Figure 10. Generally speaking, HT improve microhardness due to several strengthening mechanisms. In literature many papers are available reporting this beneficial effect, but few are available discussing the effect on MMC processed by means of AM. Similar investigations are reported in (Ref 5) on CuCrZr and in (Ref 7) on 17-4PH. These results are reported in the same Figure 10. In (Ref 25) the effect of thermal treatments on 17-4PH are discussed and it is observed that the time of treatment seems not to affect the hardness and then the estimated yield stress, while the treatment temperature does (this same behavior is observed with Cu174PH). In particular the hardness is increased from about 340 HV to 480 HV for about 500 °C treatment, while for a treatment of about 600 °C the increment is lower (up to 360 HV and then it drops down to back 340 HV after about 100 h treatment). The beneficial results of HT on Cu174PH6535 MMC are similar to those of CuCrZr but lower than those of 17-4PH. The inclusions of 17-4PH in Cu174PH6535 significantly enhances the material's mechanical properties. However, due to the high copper content, it falls short of matching the hardness level achieved by pure 17-4PH. Furthermore, it is observed that the optimal temperature value for heat treatment is 500 °C for all three materials.

The same beneficial effect of HT on Cu174PH6535 MMC is observed for thermal conductivity. In (Ref 22) the relation between composition and physical properties is discussed in terms of thermodynamics. In a crystal lattice, the atoms oscillate around their average positions with energies determined by the temperature of the solid. These atomic movements in solids are known as lattice vibrations. Various physical properties of crystals, such as specific heat and diffusivity, are associated with these atomic vibrations. The spectra of alloys differ in character from those of the pure metals and then the spectra of MMC will behave in the same way as they are a

Table 6 Thermal Conductivity measurements results

	T, °C	T, h	Volume fraction of porosity (*v2*) , -	Volume fraction of material (*v1*), -	Thermal conductivity, k , W/mK	Thermal conductivity without porosity, *k1*, W/mK
As built	0	0	…	…	44,31	…
Age Hardening	400	10	0,046	0,954	56,41	60,43
	500	10	0,033	0,967	51,36	53,92
	600	10	0,035	0,965	75,02	78,99
	700	10	0,037	0,963	57,00	60,97
	800	10	0,045	0,955	61,23	64,63
	500	5	0,040	0,960	57,48	60,98
Quenching	1000	0,5	0,025	0,975	56,38	58,50

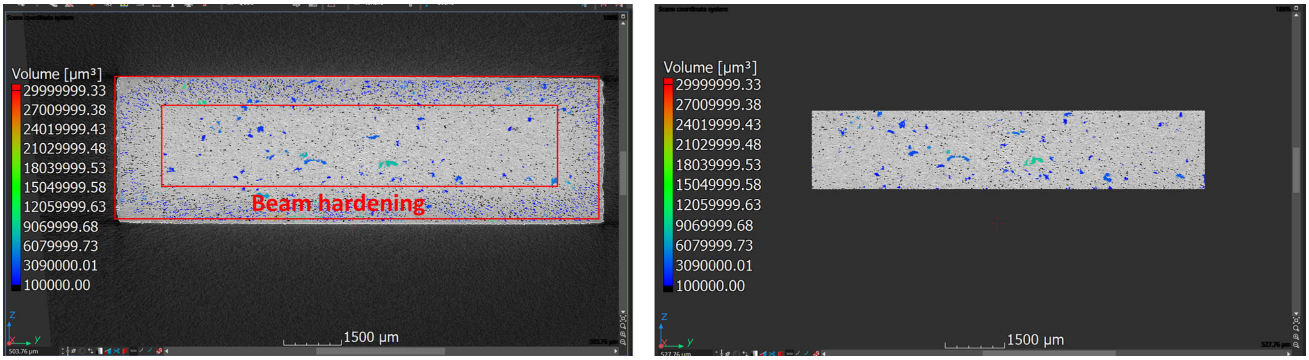

Fig. 8 CT scan acquisition

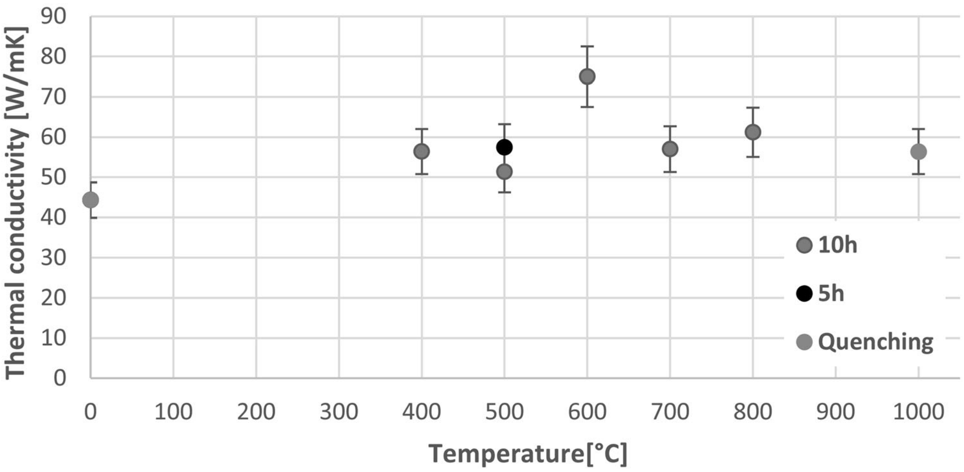

Fig. 9 Thermal Conductivity vs heat treatment temperature

composition of different alloys. Given that the HT generate different composition in the different MMC areas than the properties accordingly change. In particular in the present investigation, all HTs induce increased conductivity of the sample. In particular, the peak of conductivity for 10 h treatments is reached at 600 °C; increasing or decreasing this temperature leads to lower conductivity. The conductivity obtained at 500 °C was considered about equal to that at 400 °C because of the uncertainty of 10%, the same applies to 700 °C and 800 °C. With quenching, the lowest thermal conductivity was achieved. Reducing aging treatment to 500 °C from 10 to 5 h results in increased conductivity: probably after a certain interval of time over-aging begins. Furthermore, referring to Cu content (see Table 4) the different percentage of other than Cu elements in heat-treated specimens justifies the difference in thermal conductivity. In particular, conductivity is better for a "cleaner" Cu specimen.

The influence of HT on tensile and compressive properties confirms the increment of resistance with thermal aging. As reported in literature, as for example in (Ref 23), in MMC, the micro mechanisms of fracture are influenced by the matrix microstructure, interface characteristics, and the extent of clustering within the material. These factors are affected by heat treatments in the present MMC as pointed out by EDS and

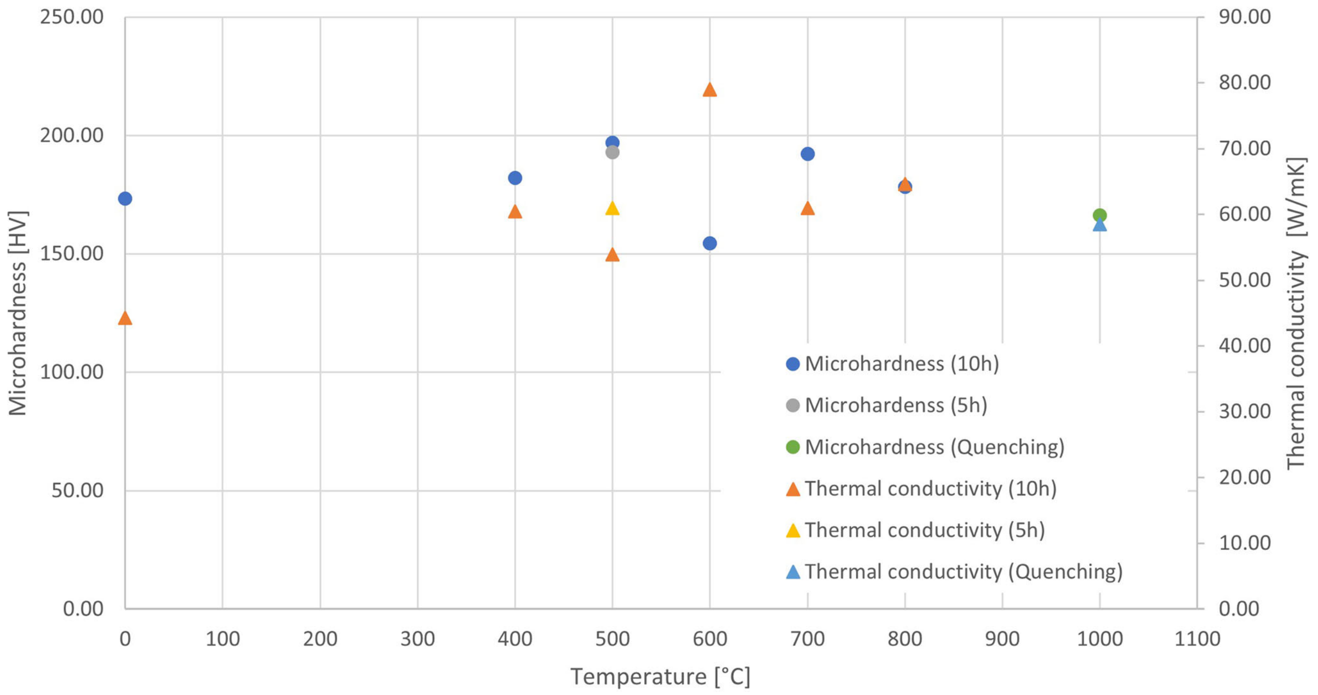

Fig. 10 Microhardness vs thermal conductivity for different heat treatments

SEM analyses which showed the variation in composition between the different zones investigated. The different mechanical properties of the zones, and in particular the Cu matrix, are affected by heat treatments basically due to solid solution structures, precipitation and various reinforcing phenomena occurring in the component materials. These kinds of influence are for example described in (Ref 24) for a Cu based alloy. In the same paper it is described the aging process causes an increment of hardness, of UTS and elongation; if elongation increment is not observed in the present case, due to steel matrix constraining effect, for what concern resistance, the prevalent contribution in the incrementing the mechanical properties of Cu is observed.

Assuming a simple rule of mixture considering the single contributions of Cu and 17-4PH components, the results obtained for Maximum stress and Failure stress can be justified.

More complex is the interpretation of Elastic modulus behavior. In (Ref 26) the increment (from 170 to 190 GPa) of the tensile Elastic modulus for a 17-4PH processed by powder extrusion and heat treated with 484 °C-1 h are reported. For what concerns pure Cu, in (Ref 27) the effect of heat treatments on Cu is reported showing dramatic decrement of Elastic modulus with heat treatments. In particular, the impact of annealing on the dynamic Young's modulus of ultrafine-grained copper, following intense plastic deformation, is examined. Isothermal annealing at temperatures up to 150 °C results to a small increment of Young's modulus, attributed mainly to a decrement of the dislocation density. Young's modulus drastically decreases when annealing at higher temperatures, ranging from 210 to 630 °C with a minimal value at 410 °C with a total decrement about 47% of the initial value and to values lower than 35% than those in the coarse-grained annealed samples. This is due to modification in the grain texture in Cu volume. In the same paper, according to Voight and Reuss model, the elastic properties of a polycrystalline body with multiple randomly oriented grains, can be estimated with mean of elastic properties of the quasi-isotropic polycrystals. In the same way we can assume to estimate the properties of the MMC assuming it as a polycrystal material with multiple randomly oriented grains with different properties. In particular, the large variability of Cu properties with heat treatment temperature affects the global behavior of the MMC.

The objective of this study was to investigate the effects of heat treatments on Cu174Ph specimens with a high number of defects. Despite the benefits observed following the heat treatments applied to Cu174Ph6535, some issues persisted, although partially mitigated by the treatments. Specifically, the material exhibited high porosity (2.5%-4.5%), as identified through CT scanning, along with the presence of voids and unmelted particles observed on the fracture surfaces of tensile specimens. These defects are likely to negatively impact the thermomechanical properties of the material and are attributed to non-ideal process parameters prior to the heat treatments. A low energy density can lead, as in this case, to an imperfect fusion of the powders (lack of fusion) (Ref 42). This results in the presence of voids, porosity, and unfused particles within the specimens. This indicates that to mitigate these defects, improvements in the fabrication process are necessary, as heat treatments alone are not sufficient.

The properties obtained for Cu174PH6535 make it particularly interesting for applications in liquid rocket engine thrust chambers. Currently, two widely used materials for such applications are CuCrZr (Ref 43) and Inconel 718 (Ref 1). When compared to Cu174PH6535, Inconel 718 exhibits superior mechanical properties, with a hardness of approximately 320 HV in the as-built condition and up to 420 HV after heat treatment (Ref 44). However, Inconel 718 has significantly lower thermal conductivity, measured at only 13.4 W/mK (Ref 45). On the other hand, the CuCrZr alloy demonstrates a hardness of approximately 85 HV in the as-built condition and a thermal conductivity of around 100 W/mK. These properties improve significantly with appropriate heat treatment: hardness reaches nearly 200 HV after aging at 500 °C for one hour, and

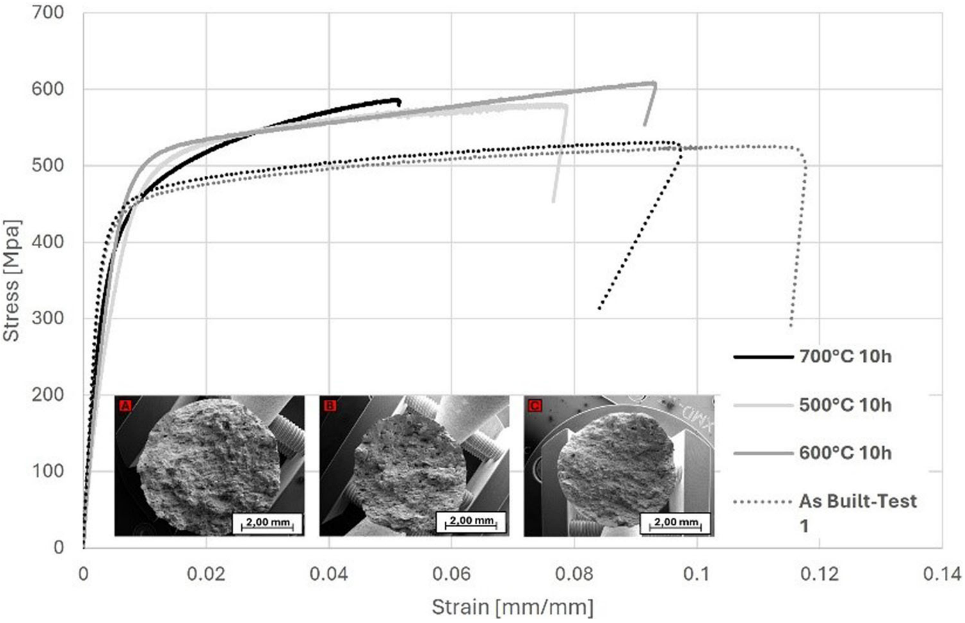

Fig. 11 Tensile Stress–Strain curve

Table 7 Tensile test results

		Strain, mm/mm	Stress, MPa	Young's Modulus, GPa
As built	Maximum	0,105	527,50	131,5
	Failure	0,097	505,00	
	Flow	…	421,25	
700–10 h	Maximum	0,051	587,11	109,15
	Failure	0,051	582,99	
	Flow	0,006	398,40	
500 °C	Maximum	0,077	580,74	63,67
	Failure	0,079	574,28	
	Flow	0,009	470,50	
600–10 h	Maximum	0,093	608,98	80,49
	Failure	0,093	605,33	
	Flow	0,008	482,90	

thermal conductivity increases to 300 W/mK after aging at 580 °C for five hours (Ref 5). In comparison, Cu174PH6535 achieves similar hardness values to CuCrZr after heat treatment, but it exhibits lower thermal conductivity. Despite this, its combination of thermal and mechanical properties, along with its manufacturability through LPBF, positions it as a promising material for demanding applications such as rocket engine thrust chambers, where both mechanical strength and thermal performance are critical.

5. Conclusions

The study investigates the effect of heat treatments on Cu174PH6535, a novel Copper-Maraging steel MMC material produced through LPBF additive manufacturing, designed to align both mechanical and thermal conductivity properties. A Design of Experiments (DoE) was employed to examine the influence of heat treatment parameters on microstructure and mechanical properties, with seven specimens subjected to varying heat treatments.

- Powder analysis revealed different particle sizes, explaining the non-homogeneous powder distribution and varying flowability of Cu and 17-4PH.
- SEM and EDS analyses highlighted the effects of heat treatments on the MMC's microstructure, demonstrating 17-4PH islands within the copper matrix and some surface porosities. EDS showed elemental migration between the matrix and islands, with heat treatments purifying the Cu matrix, improving its conductivity.
- The DoE findings indicate that treatment temperature significantly impacts conductivity and hardness. An increase in treatment temperature beyond an optimal value decrease both properties, with Cu's higher sensitivity to heat treatments driving this behavior within the tested temperature range.
- Duration effects were specifically examined for Age Hardening at 500 °C, where reducing the treatment time from 10 to 5 hours maintained similar microhardness while enhancing thermal conductivity.
- Three optimal heat treatments (500 °C for 10 h, 600 °C for 10 h, 700 °C for 10 h) were identified to balance hardness and thermal conductivity.

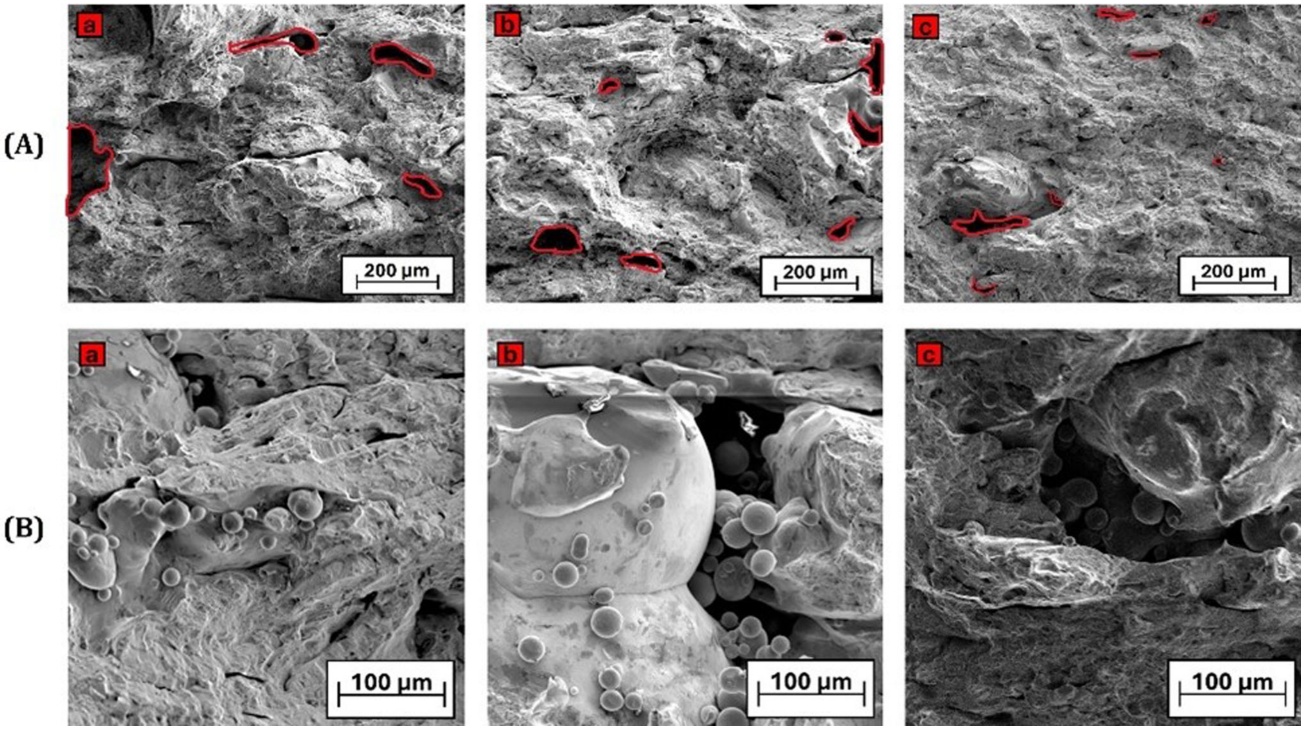

Fig. 12 Fractography (a) 700 °C–10 h; (b) 500 °C–10 h; (c) 600 °C–10 h; plane zy

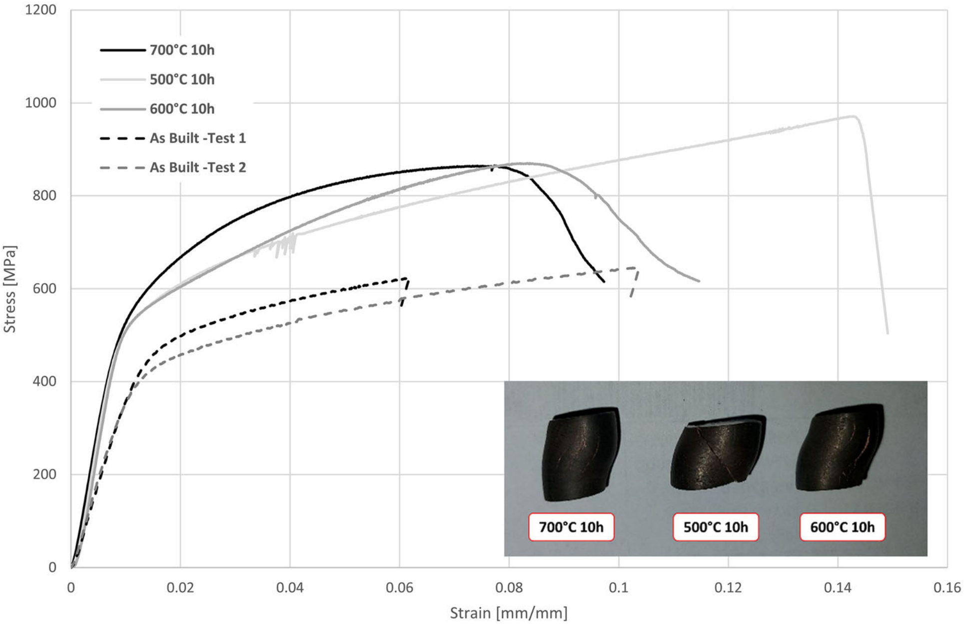

Fig. 13 Compression Stress–Strain curve. Heat Treatment

Table 8 Compression test results

	Young's modulus, GPa	Maximum Stress, MPa
As built	36,50	631,00
700 °C–10 h	65,23	864,88
500 °C–10 h	67,03	971,14
600 °C–10 h	67,27	870,15

- Compression tests revealed increased mechanical parameters post-treatment, while tensile tests showed increased yield and failure stresses, consistent with Cu alloys, alongside a decrease in Elastic modulus due to Cu's sensitivity to heat treatment.
- The study confirms the potential of Cu174PH6535 as a high-performance material in sectors such as aerospace, particularly for applications in liquid rocket engine thrust

chambers, by offering a viable alternative to traditional materials like CuCrZr and Inconel 718.

The study confirms the positive impact of heat treatments on the MMC and underscores the necessity of meticulous parameter optimization in LPBF-processed MMCs due to the multifaceted influence on critical properties.

Acknowledgments

The authors gratefully thank ASI (Italian Space Agency) for financial support of PhD research activity which led to the present results. This publication is part of the project PNRR-NGEU which has received funding from the MUR–DM 118/2023 (Fig. a)

Figa PNRR Logo

Author Contributions

Delio Lusicini contributed to conceptualization; data curation; investigation; methodology; writing—original draft. Matteo Crachi contributed to conceptualization; data curation; funding acquisition; investigation; methodology. Raffaella Sesana contributed to conceptualization; supervision; writing—review and editing. Cristiana Delprete contributed to writing—review and editing. Nicola Sicignano contributed to resources.

Funding

Open access funding provided by Politecnico di Torino within the CRUI-CARE Agreement.

Data Availability

Data will be made available on request

Conflict of interest

The authors declare that they have no known competing financial interests or personal relationships that could have appeared to influence the work reported in this paper.

Ethical Approval

Not Applicable.

Open Access

References

1. F. Kerstens, A. Cervone, and P. Gradl, End to End Process Evaluation for Additively Manufactured Liquid Rocket Engine Thrust Chambers, *Acta Astronaut.*, 2021, **182**, p 454–465.
2. B. Blakey-Milner, P. Gradl, G. Snedden, M. Brooks, J. Pitot, E. Lopez, M. Leary, F. Berto, and A. Du Plessis, Metal Additive Manufacturing in Aerospace: a Review, *Mater. Design*, 2021, **209**, 110008
3. M. Laleh, E. Sadeghi, R.I. Revilla, Q. Chao, N. Haghdadi, A.E. Hughes, W. Xu, I. De Graeve, M. Qian, I. Gibson, and M.Y. Tan, Heat Treatment for Metal Additive Manufacturing, *Prog. Mater. Sci.*, 2023, **133**, 101051
4. Rajan, T., Rajan, T., Sharma, C., Sharma, A. (2023) Heat Treatment: Principles and Techniques.101051
5. C. Wallis and B. Buchmayr, Effect of Heat Treatments on Microstructure and Properties of CuCrZr Produced by Laser-Powder Bed Fusion, *Mater. Sci. Eng. A*, 2019, **744**, p 215–223.
6. D.-H. Yang, Y.K. Kim, S.H. Park, and K.A. Lee, Improved Mechanical and Thermophysical Properties of Additively Manufactured cu-ni-sn-p Alloy by Using Aging Treatment, *J. Alloy. Compd.*, 2021, **875**, 160050
7. C.N. Hsiao, C.S. Chiou, and J.R. Yang, Aging Reactions in a 17–4 PH Stainless Steel, *Mater. Chem. Phys.*, 2002, **74**(2), p 134–142.
8. K. Kempen, E. Yasa, L. Thijs, J.-P. Kruth, and J. Van Humbeeck, Microstructure and Mechanical Properties of Selective Laser Melted 18ni-300 Steel, *Phys. Procedia*, 2011, **12**, p 255–263.
9. Contuzzi, N., Campelli, S., Casalino, G., Ludovico, A.D. (2010) Effect of heat treatment on selective laser melted steel parts
10. J. Mutua, S. Nakata, T. Onda, and Z.-C. Chen, Optimization of Selective Laser Melting Parameters and Influence of Post Heat Treatment on Microstructure and Mechanical Properties of Maraging Steel, *Mater. Design*, 2018, **139**, p 486–497.
11. S.L. Campanelli, N. Contuzzi, P. Posa, and A. Angelastro, Study of the Aging Treatment on Selective Laser Melted Maraging 300 Steel, *Mater. Res. Exp.*, 2019, **6**(6), p 066580.
12. R. Casati, J.N. Lemke, A. Tuissi, and M. Vedani, Aging Behaviour and Mechanical Performance of 18-ni 300 Steel Processed by Selective Laser Melting, *Metals*, 2016, **6**(9), p 218.
13. B. Mooney and K.I. Kourousis, A Review of Factors Affecting the Mechanical propErties of Maraging Steel 300 Fabricated Via Laser Powder Bed Fusion, *Metals*, 2020, **10**(9), p 1273.
14. Y. Sun, J. Wang, M. Li, Y. Wang, C. Li, T. Dai, M. Hao, and H. Ding, Thermal and Mechanical Properties of Selective Laser Melted and Heat Treated h13 Hot Work Tool Steel, *Mater. Design.*, 2022, **224**, p 111295.
15. Cu - PM CU101P - Powmet Legor. Powment Legor. https://legor.com/wp-content/uploads/2019/03/LegorPowmet.pdf
16. 4AR - Carpenter Additive. Carprnter additive. https://www.carpenteradditive.com/hubfs/Resources/Data%20Sheets/PowderRange 17-4% 20PH%20AR Datasheet.pdf
17. J.W. Kaczmar, K. Pietrzak, and W. Włosiński, The Production and Application of Metal Matrix Composite Materials, *J. Mater. Proc. Technol.*, 2000, **106**(1–3), p 58–67.
18. Crachi, M. (2022) "Thermo-structural analysis and associated experimental characterization of an innovative metal-matrix-composite copper-steel material for a new Liquid Rocket Engine (LRE) thrust chamber geometry processed by SLM Additive Manufacturing. M.D. Thesis, Politecnico di Torino, TO, Italy"
19. Y. Lu, S. Wu, Y. Gan, T. Huang, C. Yang, L. Junjie, and J. Lin, Study on the Microstructure, Mechanical Property and Residual Stress of SLM Inconel-718 Alloy Manufactured by Differing Island Scanning Strategy, *Opt. Laser Technol.*, 2015, **75**, p 197–206.
20. Slotwinski, J., Moylan, S. (2014) Applicability of existing materials testing standards for additive manufacturing materials https://doi.org/10.6028/NIST.IR.8005
21. A.Y. Kumar, J. Wang, Y. Bai, S.T. Huxtable, and C.B. Williams, Impacts of Process-Induced Porosity on Material Properties of Copper Made by Binder Jetting Additive Manufacturing, *Mater. Design.*, 2019, **182**, p 108001.
22. Vora, A.M. (2008) Lattice Dynamics of Solid Metallic Elements, p.103. Nova Science Publisher, Inc

23. J.J. Lewandowski, C. Liu, and W.H. Hunt, Effects of Matrix Microstructure and Particle Distribution on Fracture of an Aluminum metal Matrix Composite, *Mater. Sci. Eng.*, 1989, **107**, p 241–255.
24. Q. Wang, Y. Zhang, K. Wang, S. Liu, X. Zhang, and H. Shao, Effect of Process Parameters and Heat Treatment on the Microstructure and Properties of CuCrZr Alloy by Selective Laser Melting, *Mater. Sci. Eng.*, 2022, **857**, 144054
25. G. Yeli, M.A. Auger, K. Wilford, G.D. Smith, P.A. Bagot, and M.P. Moody, Sequential Nucleation of Phases in a 17–4PH Steel: Microstructural Characterisation and Mechanical Properties, *Acta Mater.*, 2017, **125**, p 38–49.
26. J. Jones, A. Vafadar, and R. Hashemi, A Review of the Mechanical Properties of 17–4PH Stainless Steel Produced by Bound Powder Extrusion, *J. Manuf. Mater. Proc.*, 2023, **7**(5), p 162.
27. P. Pal-Val, L. Pal-Val, V. Natsik, A. Davydenko, and A. Rybalko, Giant Young'S Modulus Variations in Ultrafine-Grained Copper Caused by Texture Changes at Post-Spd Heat Treatment / Gigantyczne Zmiany Modułu Younga W Ultra Drobnoziarnistej Miedzi Spowodowane Przez Zmiany Tekstury W Trakcie Obróbki Cieplnej Po SPD, *Archiv. Metall. Mater.*, 2015, **60**(4), p 3073–3076. https://doi.org/10.1515/amm-2015-0491
28. C.L. Kugelmeier, L.F. Unti, E.L. Júnior, N.M. Souza, A.L. Jardini, J.A. Avila, O.M. Cintho, and K. Zilnyk, Microstructure Evolution and Corrosion Resistance Evaluation of 17–4 Precipitation Hardening Stainless Steel Processed by Laser Powder Bed Fusion, *J. Mater. Eng. Perform.*, 2024, **2**, p 1–1.
29. F.F. Conde, J.A. Avila, J.P. Oliveira, N. Schell, M.F. Oliveira, and J.D. Escobar, Effect of the as-Built Microstructure on the Martensite to Austenite Transformation in a 18Ni Maraging Steel After Laser-Based Powder Bed Fusion, *Addit. Manufact.*, 2021, **46**, p 102122.
30. M.P. Behera, T. Dougherty, and S. Singamneni, Conventional and Additive Manufacturing with Metal Matrix Composites: A Perspective, *Proc. Manufact.*, 2019, **30**, p 159–166.
31. N. Li, W. Liu, Y. Wang, Z. Zhao, T. Yan, G. Zhang, and H. Xiong, Laser Additive Manufacturing on Metal Matrix Composites: A Review, *Chin. J. Mech. Eng.*, 2021, **34**, p 1–6.
32. J. Shi and Y. Wang, Development of Metal Matrix Composites by Laser-Assisted Additive Manufacturing Technologies: a Review, *J. Mater. Sci.*, 2020, **55**(23), p 9883–9917.
33. A.I. Mertens, Metal matrix composites processed by laser additive manufacturing, *additive manufacturing*. Elsevier, 2021, p 409–425. https://doi.org/10.1016/B978-0-12-818411-0.00005-7
34. B. AlMangour and J.M. Yang, Integration of Heat Treatment with Shot Peening of 17–4 Stainless Steel Fabricated by Direct Metal Laser Sintering, *Jom.*, 2017, **69**, p 2309–2313.
35. B. AlMangour and J.M. Yang, Understanding the Deformation Behavior of 17–4 Precipitate Hardenable Stainless Steel Produced by Direct Metal Laser Sintering Using Micropillar Compression and TEM, *Int. J. Adv. Manuf. Technol.*, 2017, **90**, p 119–126.
36. Y. Liu, M. Tang, Q. Hu, Y. Zhang, and L. Zhang, Densification Behavior, Microstructural Evolution, and Mechanical Properties of TiC/AISI420 Stainless Steel Composites Fabricated by Selective Laser Melting, *Mater. Design.*, 2020, **187**, p 108381.
37. P.L. Santos, J.A. Avila, E.B. da Fonseca, A.H. Gabriel, A.L. Jardini, and É.S. Lopes, Plane-Strain Fracture Toughness of Thin Additively Manufactured Maraging Steel Samples, *Add. Manuf.*, 2022, **49**, p 102509. https://doi.org/10.1016/j.addma.2021.102509
38. E.B. Fonseca et al., Fracture Toughness and Wear Resistance of Heat-Treated H13 Tool Steel Processed by Laser Powder Bed Fusion, *Addit. Manuf.*, 2023, **78**, p 103862. https://doi.org/10.1016/j.addma.2023.103862
39. B. AlMangour, Y.K. Kim, D. Grzesiak, and K.A. Lee, Novel TiB2-Reinforced 316L Stainless Steel Nanocomposites with Excellent Room-and High-Temperature Yield Strength Developed by Additive Manufacturing, *Composit. Part B: Eng.*, 2019, **156**, p 51–63. https://doi.org/10.1016/j.compositesb.2018.07.050
40. Y. Hu and W. Cong, A Review on Laser Deposition-Additive Manufacturing of Ceramics and Ceramic Reinforced Metal Matrix Composites, *Ceramics Int.*., 2018, **44**(17), p 20599–20612. https://doi.org/10.1016/j.ceramint.2018.08.083
41. B. AlMangour, *Additive Manufacturing of Emerging Materials*, Springer, Cham, 2019. https://doi.org/10.1007/978-3-319-91713-9
42. S. Qu, J. Ding, J. Fu, M. Fu, B. Zhang, and X. Song, High-Precision Laser Powder Bed Fusion Processing of Pure Copper, *Addit. Manuf.*, 2021, **48**, p 102417.
43. K. Morshed-Behbahani et al., Additive Manufacturing of Copper-Based Alloys for High-Temperature Aerospace Applications: a Review, *Mater. Today Commun.*, 2024, **38**, 108395
44. E. Hosseini and V.A. Popovich, A Review of Mechanical Properties of Additively Manufactured Inconel 718, *Addit. Manuf.*, 2019, **30**, 100877
45. Q. Yin et al., Improving Thermal Conductivity of Inconel 718 Through Thermoelectric Coupling to Reduce Cutting Temperature, *J. Market. Res.*, 2022, **20**, p 950–957.